Numerical Study of the Intensity Correlation between Secondary Flow and Heat Transfer of Circle Tube-Finned Heat Exchanger with Vortex Generators

Yong Guan[1], Wanling Hu[1, 2, *], Yun Zhang[1], Kewei Song[2, 3] and Liangbi Wang[2, 3]

Abstract: The application of vortex generators in tube-finned heat exchangers is very universal. The vortex generators can generate secondary flow, and as we all know secondary flow can obviously strengthen heat transfer. To use vortex generators much more efficiently in the circle tube-finned heat exchangers, the intensity correlation study between secondary flow and heat transfer is needed. 22 different structures of circle tube-finned heat exchangers were numerically studied, including the plain fin cases and the cases with vortex generators. In addition, the influence of fin spacing, transverse and longitudinal tube pitch, heights and attack angle of vortex generators, positions of vortex generators and shape of vortex generators on heat transfer and fluid flow are studied, too. The non-dimensional parameter *Se* is applied to quantify the secondary flow intensity. The results show that *Se* can describe the secondary flow intensity very well. There is very close corresponding relationship between overall averaged *Nu* and volumetrically averaged *Se* for all the researched cases and the relational expression is obtained. However, there is no one-to-one correlation not only between *Re* and *f* but also between volumetrically averaged *Se* and *f* for all the studied cases.

Keywords: Enhanced heat transfer, numerical analysis, quantitative relationship, secondary flow.

Nomenclature

A	Cross-sectional area (m^2)
$A(x)$	Cross-sectional area at the x coordinate (m^2)
c_p	Specific heat (J/(kg K))
D	Outer diameter of tube (m)
d_e	Equivalent diameter (m)
f	Friction factor

[1] School of Environmental and Municipal Engineering, Lanzhou Jiaotong University, Lanzhou, China.

[2] Key Laboratory of Railway Vehicle Thermal Engineering (Lanzhou Jiaotong University), Ministry of Education of China, Lanzhou, China.

[3] Department of Mechanical Engineering, Lanzhou Jiaotong University, Lanzhou, China.

[*] Corresponding Author: Wanling Hu. Email: huwanlling@mail.lzjtu.cn.

Received: 14 November 2019; Accepted: 23 December 2019.

H_1,H_2	Height of vortex generator (m)
L	Length of vortex generator (m)
L_x	Stream wise length of fin (m)
n	Normal direction
Nu	Nusselt number
p	Pressure (Pa)
Re	Reynolds number
S	Total heat transfer surface (m^2)
S_1	Transversal tube pitch (m)
S_2	Longitudinal tube pitch (m)
Se	Non-dimension parameter describing the intensity of secondary flow
$S(x)$	Spanning strip of heat transfer surface at x coordinate
T_{p}	Net fin spacing (m)
T	Temperature (K)
$u_{\max}$	Maximum average velocity of cross section (m/s)
u_{i}, u, v, w	Velocity components (m/s)
X_1, Y_1	Position parameters of vortex generator (m)
Δp	Pressure drop (Pa)

Greeks

λ	Thermal conductivity (W/(m K))
μ	Viscosity (kg/(m s))
ρ	Density (kg/m^3)
θ	Attack angle (°)
ω	Vorticity (1/s)

Subscripts

in	Inlet parameters
local	Local value
s	Span-averaged value
out	Outlet parameters
w	Solid wall surface

1 Introduction

Tube-finned heat exchangers are widely applied in many fields, such as chemical industry, transportation, and air conditioning & refrigeration systems. The development of tube-finned heat exchangers with high efficiency and energy saving has significant application value. It is well known that the thermal characteristic of these kinds of tube-finned heat exchanger is mainly limited by the airside heat transfer coefficient due to its higher thermal resistance. To reduce the airside thermal resistance of tube-finned heat exchangers, it is a very effective way to introduce vortex generators (VGs) in the tube-finned heat exchangers [Fiebig (1995)]. The key mechanism of heat transfer enhancement using VGs is that the VGs can contribute to longitudinal vortices in its mainstream direction and disrupt the thermal boundary laye [Fiebig, Valencia and Mitra (1994)].

In recent years, a great quantity of studies about the use of VGs to enhance heat transfer of tube-finned heat exchangers was performed. ElSherbini et al. [ElSherbini and Jacobi (2002)] studied experimentally the effectiveness of delta-wing VGs applied to tube-finned heat exchangers. They found that Colburn factor increases 31% over the baseline at Reynolds numbers from about 700 to 2300 and without any pressure drop penalties. Zhang et al. [Zhang, Wang and Yang (2003)] used naphthalene sublimation mass and heat analogy experiment to analyze the effect of attack angle θ, shape angle β and span Δy of a vortex generator on the local heat transfer of a round tube-finned heat exchanger. The results showed that Nu increased with increasing of θ and decreasing of β, and Nu was obviously enhanced under a smaller span of the vortex generator. Gao et al. [Gao, Wang, Zhang et al. (2003)] and Ke et al. [Ke, Wang, Hua et al. (2006)] investigated the heat transfer of a flat tube-finned heat exchanger with VGs and found the optimal height and attack angle of VGs, respectively. Lemouedda et al. [Lemouedda, Breuer, Franz et al. (2010)] investigated and presented the optimal angles of attack of VGs in tube-finned heat exchangers. Numerical simulation study on heat transfer enhancement using winglet VG arrays and rectangular winglet pairs in tube-finned heat exchangers was implemented by He et al. [He, Han, Tao et al. (2012); He, Chu, Tao et al. (2013)]. The effects of attack angle of VGs and the layout locations were examined. The optimal fin spacing and transverse tube pitch of circle tube-finned heat exchanger with VGs at different front inlet velocity were found by Hu et al. [Hu, Su, Wang et al. (2013); Hu, Wang and Guan (2015)]. Delač et al. [Delač, Trp and Lenić (2014)] analysed the influence of impact angles and height of winglet VGs on the heat transfer and fluid flow performance of flat tube-finned heat exchanger with VGs. The influence of main geometric parameters of the curved delta VGs and curved rectangular VGs on the flow resistance and heat transfer performance of circle tube-finned heat exchanger was investigated numerically by Gong et al. [Gong, Wang and Lin (2015)] and Lin et al. [Lin, Liu, Lin et al. (2015)], respectively. Through simulated numerically, Salviano et al. [Salviano, Dezan and Yanagihara (2016)] found an optimum configuration of the VGs from seven independent parameters for VGs using Colburn and Friction factor. Behfard et al. [Behfard and Sohankar (2016)] studied the effect of height and length of VGs, longitudinal and transverse positions of VGs, and the attack angle of delta winglet VGs on the thermal characteristics of the tube-finned heat exchanger. They found that comparing with the geometry without VGs, convective heat transfer ratio of the best model were increased by 59%. Experimental research of the heat transfer of circular tube-finned heat exchanger with VGs under different geometric sizes was carried out by Song et al. [Song, Xi, Su et al. (2017)]. They found the optimal fin spacing, tube pitch and VG sizes. Sarangi et al. [Sarangi and Mishra (2017)] investigated the effects of VGs number, location and attack angle on heat transfer of a tube-finned heat exchanger with rectangular VG pairs in detail. Qian et al. [Qian, Wang and Cheng (2018)] numerically studied the effect of length, angle and height of rectangle-winglet VGs on heat transfer and fluid flow performance of tube-finned heat exchanger with rectangle-winglet VGs. Awais et al. [Awais and Bhuiyan (2019)] discussed the effect of VGs with different number of rows, attack angles, configuration and different tube arrangements on heat transfer performance and pressure drop of compact tube-finned heat exchangers. And the optimal values of the corresponding parameters were obtained. The effect of different VG geometries and different arrangements in a tube-finned heat exchanger was investigated by Salleh et al. [Salleh, Gholami and Wahid (2019)] using numerical simulation method. They found that the best heat transfer performance was given by delta winglet VGs in common flow up arrangement.

Above mentioned studies mainly focus on the effect of structural parameters and arrangement variation of VGs and tubes on thermal and hydrodynamic performance of tube-finned heat exchangers. The purpose is to obtain the optimal structure parameters of vortex generator and heat exchanger, so as to improve the thermal and hydrodynamic performance of the tube-finned heat exchanger. The reason why VGs are so extensively studied is that it is generally known that VGs can generate secondary flow and the secondary flow can obviously increase the heat transfer capacity of tube-finned heat exchangers. However, the precise quantitative correlation between secondary flow intensity and heat transfer intensity in tube-finned heat exchanger with VGs is seldom studied. For more efficient use of secondary flow, it is necessary to study the quantitative correlation between secondary flow intensity and heat transfer intensity.

In order to obtain the quantitative correlation between secondary flow intensity and heat transfer intensity, it is essential to find an appropriate parameter to describe the secondary flow intensity. Although the absolute vortex flux J^{n}_{ABS} reported by Chang et al. [Chang, Wang, Song et al. (2009)] and Lin et al. [Lin, Sun and Wang (2009)] is more universally applicable than Dean number [Moulin, Rouch, Serra et al. (1996)] and the swirl parameter [Manglik and Bergles (1993)], it is difficult to find an accurate quantitative correlation between the absolute vortex flux J^{n}_{ABS} and convective heat transfer coefficient h or Nusselt number.

Therefore, a dimensionless parameter *Se* was defined by Song et al. [Song and Wang (2013)] to specify the secondary flow intensity. Since *Se* was defined, it is possible to determine the quantitative correlation between the secondary flow intensity and heat transfer intensity of tube-finned heat exchanger. Hu et al. [Hu, Song, Guan et al. (2013)] studied the relationship between secondary flow intensity and heat transfer intensity of circle tube-finned heat exchanger with delta winglet VGs at different fin spacing, height and attack angle of VGs. The results showed that Nusselt number has closely corresponding relationship with *Se* for the studied cases. Gong et al. [Gong, Wang and Lin (2015)] and Lin et al. [Lin, Liu, Lin et al. (2015)] also found that Nusselt number has a very close corresponding relationship with *Se* for the circle tube-finned heat exchanger with the curved delta VGs and curved rectangular VGs, respectively. In addition, the exact quantitative correlation between Nusselt number and *Se* in flat tube-finned heat exchanger with VGs was found by Song et al. [Song, Hu, Liu et al. (2016)].

Although the corresponding relationship between the secondary flow intensity and heat transfer intensity of tube-finned heat exchanger was found in the above mentioned papers, the approximate formula between *Se* and *Nu* is only apply to the simple structural parameters that studied in the published papers. Because the variable parameters of structure and arrangement in the tube-finned heat exchanger with VGs are numerous, does the strong corresponding relationship between *Nu* and *Se* still exist when the structural parameters change? How about the relationship between *Se* and friction factor *f*? So, more studies about the corresponding relationship between secondary flow intensity and heat transfer intensity, flow resistance of different configurations in tube-finned heat exchangers are required.

To obtain the quantitative correlation between secondary flow intensity and heat transfer intensity, the heat transfer and secondary flow characteristics of circle tube-finned heat exchanger with 22 different configurations, that is, different fin spacing, different transverse and longitudinal tube pitch, different height of VGs, different attack angle of VGs, different position of VGs and different shape of VGs were numerically studied in detail. The results can help us to utilize longitudinal vortices produced by VGs more effectively in the circle tube-finned heat exchanger.

2 Physical model

Schematic diagram of a four-row circle tube-finned heat exchanger with VGs is given in Fig. 1. The locations of the circle tubes and the VGs are indicated in Fig. 2(a). As we can see, the circle tubes and the VGs in the heat exchanger are symmetrically distributed. In order to save computation time and storage space, a symmetrical unit of the shadow area in the tube-finned heat exchanger is selected as the computational domain. As shown in Fig. 2(a), the region A-B-C-D-E-F-G-H-I-J-K-L-A is the computational domain used in the paper. The boundaries AB, CD, EF, GH, IJ, and KL are all symmetric surfaces. In addition, three different shapes of VGs shown in Fig. 2(b) are studied. The studied 22 different structures with different fin spacing, different transverse and longitudinal tube pitch, different height of VGs and attack angle of VGs, different position of VGs and different shape of VGs are presented in Tab. 1. From Fig. 3, we can see the 3D structure diagram of the computational domain.

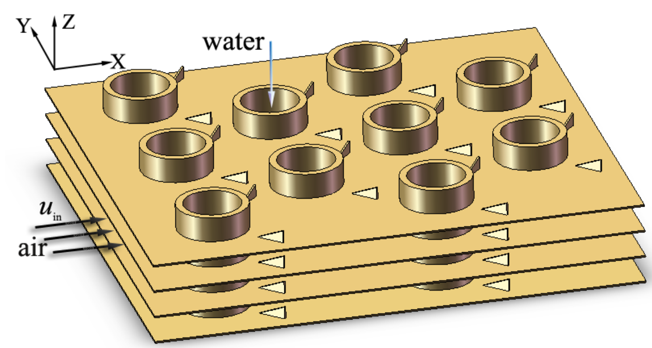

Figure 1: Sketch map of a circle tube-finned heat exchanger with VGs

Table 1: Geometric parameters of researched cases

Case	D (mm)	T_p (mm)	X_1 (mm)	Y_1 (mm)	H_1 (mm)	H_2 (mm)	L (mm)	θ (o)	S_1 (mm)	S_2 (mm)	Adopted grid size
C1	10	1.5	/	/	/	/	/	/	20	15.5	239×55×17
C2	10	2	/	/	/	/	/	/	20	15.5	239×55×22
C3	10	2.5	/	/	/	/	/	/	20	15.5	239×55×27
C4	10	1.5	5	5	/	1.500	3.0	35	20	15.5	239×55×17
C5	10	2	5	5	/	1.500	3.0	35	20	15.5	239×55×22
C6	10	2.5	5	5	/	1.500	3.0	35	20	15.5	239×55×27
C7	10	2	5	5	/	1.750	3.5	35	20	15.5	247×55×24
C8	10	2	5	5	/	2.000	4.0	35	20	15.5	245×55×21
C9	10	2	5	5	/	1.750	3.5	20	20	15.5	181×61×22
C10	10	2	5	5	/	1.750	3.5	45	20	15.5	259×59×23
C11	10	2	5	5	/	1.750	3.5	35	17	15.5	247×47×24
C12	10	2	5	5	/	1.750	3.5	35	23	15.5	247×65×24
C13	10	2	5	5	/	1.750	3.5	35	28	15.5	247×69×24
C14	10	2	5	5	/	1.750	3.5	35	20	13.5	215×55×24
C15	10	2	5	5	/	1.750	3.5	35	20	20.0	303×55×24
C16	10	2	5	5	/	1.750	3.5	35	20	23.0	351×55×24
C17	10	2	5	5	0.8750	0.875	3.5	35	20	15.5	247×55×24
C18	10	2	5	5	0.4375	1.313	3.5	35	20	15.5	247×55×24
C19	10	2	5	5	0.5830	1.167	3.5	35	20	15.5	247×55×24
C20	10	2	5	2.5	/	1.750	3.5	35	20	15.5	247×55×24
C21	10	2	5	7.5	/	1.750	3.5	35	20	15.5	247×55×24
C22	10	2	7.5	5	/	1.750	3.5	35	20	15.5	247×55×24

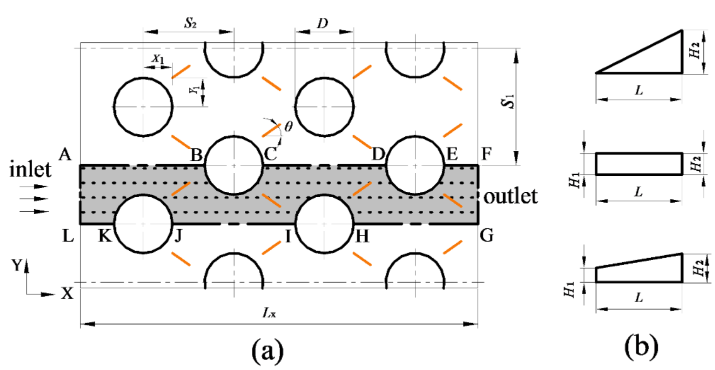

Figure 2: The structure of the fin and VGs: (a) locations of the circle tubes and the VGs and determination of symmetrical boundaries; (b) shapes of VGs

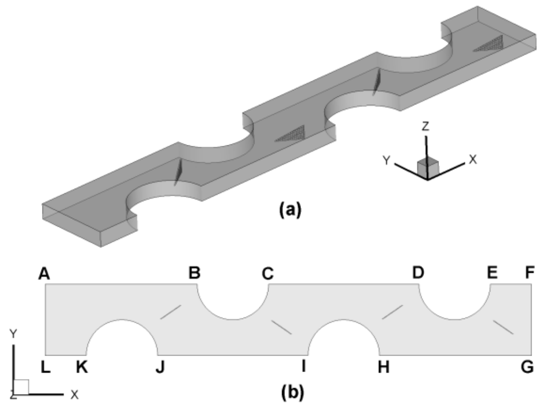

Figure 3: Structure diagram of computational domain: (a) 3D view; (b) X-Y plane projection view

3 Mathematical formulation

3.1 Governing equations

As reported in Song et al. [Song, Hu, Liu et al. (2016)], under the rated working condition, the air velocity at inlet of intercoolers is about 7.22 m/s. The flow can be assumed as a laminar flow and the fluid is incompressible. In this paper, the maximum air velocity at inlet that studied is less than 7.22 m/s, that is, *Re* is less than 1800 for all the studied cases. In addition, the air inlet temperature is 40°C, and the surface temperature of the tube and fin is 60°C. The physical properties of the air are considered to be constant and the viscous dissipation can be neglected. The three conservation equations in the computational domain are:

$$\frac{\partial}{\partial x_i}(\rho u_i) = 0 \tag{1}$$

$$\frac{\partial}{\partial x_i}(\rho u_i u_k) = \frac{\partial}{\partial x_i}(\mu \frac{\partial u_k}{\partial x_i}) - \frac{\partial p}{\partial x_k} \quad (k = 1,2,3) \tag{2}$$

$$\frac{\partial}{\partial x_i}(\rho c_p u_i T) = \frac{\partial}{\partial x_i}(\lambda \frac{\partial T}{\partial x_i}) \tag{3}$$

3.2 Boundary conditions

The inlet section boundary:

$$u(x,y,z)\big|_{\text{in}} = u_{\text{in}} ,\ v(x,y,z)\big|_{\text{in}} = 0 ,\ w(x,y,z)\big|_{\text{in}} = 0 ,\ T(x,y,z)\big|_{\text{in}} = T_{\text{in}} \tag{4}$$

The outlet section boundary is same as adopted in Hu et al. [Hu, Su, Wang et al. (2013)]:

$$\begin{aligned} &u(x,y,z)\big|_{\text{out}} = u(x_*, S_1/2 - y, z), (u(x,y,z) < 0) \\ &\frac{\partial u(x,y,z)}{\partial n}\big|_{\text{out}} = 0, (u(x,y,z) > 0) \end{aligned} \tag{5}$$

$$\frac{\partial v(x,y,z)}{\partial n}\Big|_{\text{out}}=0, \quad \frac{\partial w(x,y,z)}{\partial n}\Big|_{\text{out}}=0, \quad \frac{\partial T(x,y,z)}{\partial n}\Big|_{\text{out}}=0 \tag{6}$$

The symmetric surfaces boundary:

$$\frac{\partial u(x,y,z)}{\partial n}=0, \quad v(x,y,z)=0, \quad \frac{\partial w(x,y,z)}{\partial n}=0, \quad \frac{\partial T(x,y,z)}{\partial n}=0 \tag{7}$$

The solid surfaces boundary:

$$u(x,y,z)=0, \quad v(x,y,z)=0, \quad w(x,y,z)=0, \quad T=T_{\text{w}} \tag{8}$$

3.3 Parameter definition

The Reynolds number is:

$$Re=\rho u_{\max} d_{\text{e}} / \mu \tag{9}$$

The friction factor is:

$$f=\Delta p d_{\text{e}} / \left(L_x \rho u_{\max}^2 / 2\right) \tag{10}$$

where $L_x = x_F - x_A$, as given in Fig. 3(b).

The equivalent diameter is selected same as adopted in Zhang et al. [Zhang, Wu and Wang (2008)]:

$$d_{\text{e}}=4F_{\text{C}}L_x / F' \tag{11}$$

where F_C is the smallest cross-sectional area, F' is the total heat transfer surfaces area.

The local Nusselt number is defined as:

$$Nu_{\text{local}}=\left(-d_{\text{e}}\frac{\partial T}{\partial n}\right)_{\text{w}} / (T_{\text{w}}-T_{\text{ave}}) \tag{12}$$

where, $T_{ave}=(T_{\text{in}}+T_{\text{out}})/2$, T_{in} and T_{out} are the cross-section averaged temperature of the inlet and outlet, respectively [Wang, Su, Hu et al. (2011)].

The crosswise averaged Nu_s is obtained by calculating the average value of Nu_{local} on the spanning strips of the fins and the tube surfaces at x coordinates:

$$Nu_{\text{s}}(x)=\iint\limits_{S(x)} Nu_{\text{local}} dS / \iint\limits_{S(x)} dS \tag{13}$$

The overall averaged Nu is defined as:

$$Nu=\iint\limits_{S} Nu_{\text{local}} dS \Big/ \iint\limits_{S} dS \tag{14}$$

where S is all the heat transfer surfaces included in the computational domain:

A non-dimensional parameter Se used to quantify the secondary flow intensity is defined in Song et al. [Song and Wang (2013)].

$$Se=\frac{\rho d_{\text{e}} U_{\text{s}}}{\mu} \tag{15}$$

where

$$U_{\mathrm{s}} = \frac{d_{\mathrm{e}}}{A(x)} \iint_{A(x)} \left|\omega^n\right| dA \tag{16}$$

The cross section averaged Se_{s} is:

$$Se_s(x) = \frac{\rho d_{\mathrm{e}}^2}{\mu} \iint_{A(x)} \left|\omega^n\right| dAdx \Big/ \iint_{A(x)} dAdx \tag{17}$$

The volumetrically averaged Se is obtained by integrating the local Se over the entire flow field in the computational domain:

$$Se = \frac{\rho d_{\mathrm{e}}^{\ 2}}{\mu} \iiint_V \left|\omega^n\right| dV \Big/ \iiint_V dV \tag{18}$$

4 Numerical method

The numerical simulation method applied in this paper is the same as that used in Hu et al. [Hu, Su, Wang et al. (2013); Hu, Wang and Guan (2015)]. Grid dependency verification was performed on three fin spacing cases with delta winglet VGs at Re=1134, H_2=1.5 mm and θ=35°. The grid sizes used for grid independence check were given in Tab. 2. The maximum deviation of average Nu is 1.2%. The maximum deviation of f is 1.5%. Therefore, the grid dependence is good. To save computational time and ensure calculation accuracy, the adopted grid size in the computational domain is 239×55×17, 239×55×22 and 239×55×27 for the three different fin spacing cases, respectively. For the other different models simulated, the mesh size will be adjusted appropriately. The adopted grid sizes of all the cases that studied were given in Tab. 1. The sketch of grid system is presented in Fig. 4.

Table 2: The adopted grid sizes of the cases

T_{p} (mm)	Case	Grid size	Nu	f
		186×40×14	6.5953	0.1217
1.5	C4	239×55×17	6.5855	0.1233
		330×82×26	6.5134	0.1214
		186×40×18	7.1628	0.1347
2.0	C5	239×55×22	7.1929	0.1358
		330×82×34	7.1952	0.1360
		186×40×21	7.4645	0.1506
2.5	C6	239×55×27	7.5319	0.1528
		330×82×40	7.5444	0.1518

Validation of numerical results with condensation experimental results presented in Zhang et al. [Zhang, Wu and Wang (2008)] under the same structural parameters is given in Fig. 5. As shown in Fig. 5, the numerical results agree well with the experimental results. From Fig. 5(a), we can get the maximum discrepancy of Nu between numerical results with experimental data is 16.7%. The maximum discrepancy of f is 6.5% as shown in Fig. 5(b). These further illustrate that the adopted numerical methods are reliable.

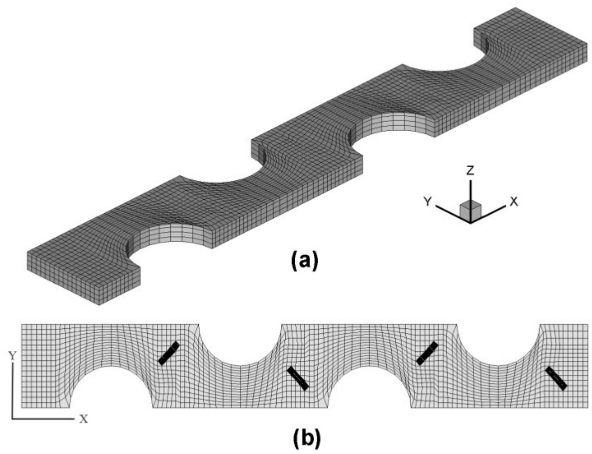

Figure 4: The sketch of grid system: (a) three-dimensional view; (b) X-Y plane projection view

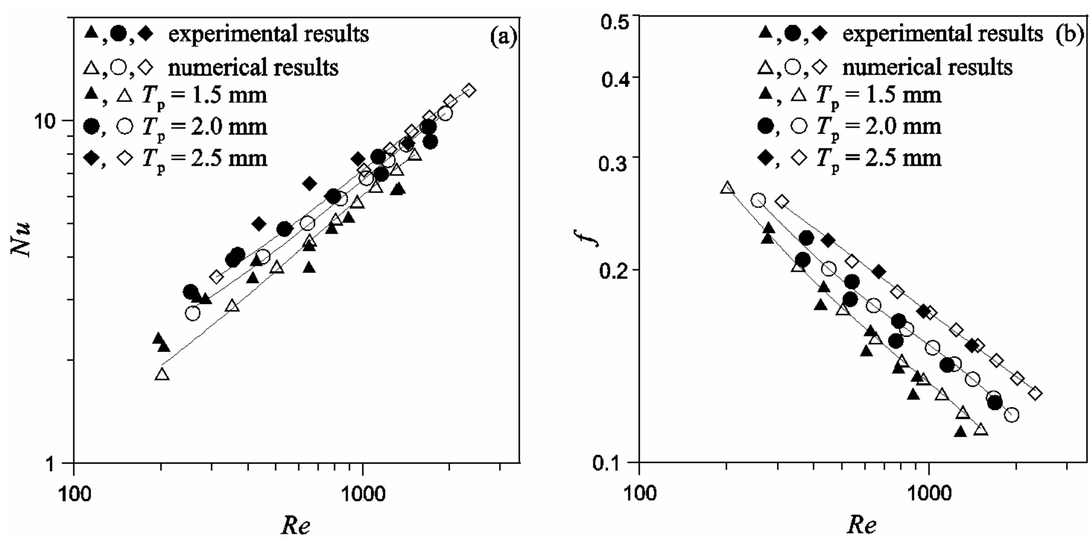

Figure 5: Validation of numerical results with experimental data: (a) *Re* and *Nu*; (b) *Re* and *f*

5 Results and discussions

5.1 Comparisons Se and secondary flow intensity

In order to show that *Se* is well connected with the secondary flow intensity, Figs. 7 and 8 show the velocity fields and distributions of *Se* at the nine transverse sections which locations are given in Fig. 6 for the case with delta winglet VGs at S_1=20 mm, S_2=15.5

mm, T_p=2 mm, H_2=1.75 mm, θ=35° under Re=1134. For the convenience of comparison, the corresponding cross sections without VGs is also given.

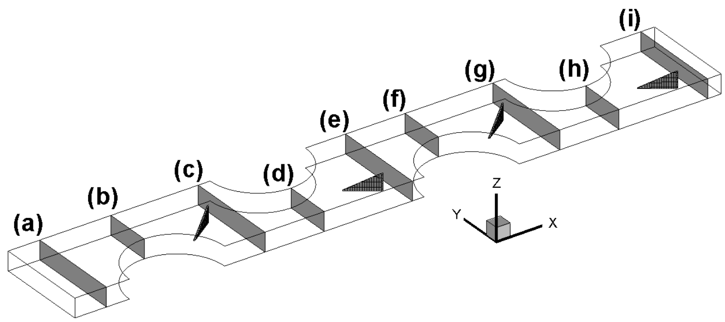

Figure 6: The locations of the nine cross sections indicated in Figs. 7 and 8

Fig. 7 shows secondary flow distribution of each section which shown in Fig. 6. The left column of Fig. 7 shows secondary flow of circle tube-finned heat transfer without VGs, the right column shows secondary flow of circle tube-finned heat transfer with VGs. The development of longitudinal vortices in the circle tube-finned heat transfer can be clearly seen from these secondary flow distribution fields. Comparing the corresponding section secondary flow of the left and right columns, it is clear that except Figs. 7(a) and 7(b) which situated at the front of the first VG, secondary flow intensity of the right column is stronger than that of the left column. This means that the introduction of the VGs strengthens the longitudinal vortex of the channel. From Fig. 7(a), we can see that the secondary flow on this section is very weak, because this section is near the inlet region, secondary flow has not been developed. As shown in Fig. 7(b), because of the existence of the circular tube, the flow cross-section area changes, secondary flow is developing. Because the flow at the location showed in Figs. 7(a) and 7(b) has not been influenced by VGs strongly, the distributions of secondary flow are similar for both left column and right column. As depicted in Fig. 7(c), due to the introduction of VGs, vortices are generated; the secondary flow is strengthened on the section of the right column. Fig. 7(d) shows that the secondary flow generated by the combined action of the circle tube and VGs is much stronger than that without VGs. On the sections behind the VGs, as shown in Figs. 7(e) to 7(h), the secondary flow distribution has the similar characteristics as that shown in Figs. 7(c) and 7(d). The direction of secondary flow distribution after the second VG depicted in Figs. 7(e) and 7(f) is opposite to Figs. 7(c) and 7(d). In the section behind the forth VG, as shown in Fig. 7(i), the secondary flow intensity generated by the last VG is smaller than that generated by the other VGs.

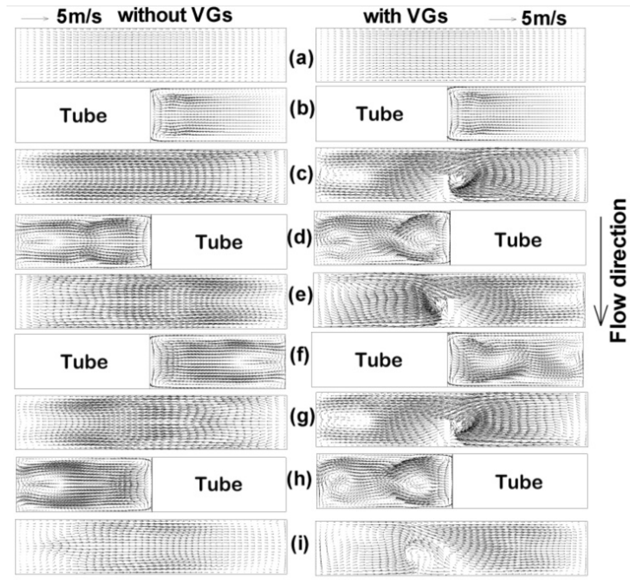

Figure 7: Velocity fields on the different cross sections shown in Fig. 6 at *Re*=1134

The fields of *Se* of each section shown in Fig. 6 are depicted in Fig. 8. The left column of this figure shows the case without VGs, the right column shows the case with VGs. It can be clearly seen that the *Se* distribution of the left and right columns are different, *Se* is enhanced by VGs on all cross sections except the two cross sections showed in Figs. 8(a) and 8(b). Fig. 8(a) shows that the value of *Se* on the section is small. From Fig. 8(b), we can see that at the middle sections of the first tube, large *Se* exists near the tube because of the horseshoe vortex produced by the circular tube. In the section behind the first VG shown in Fig. 8(c), because of the existence of the VG, the secondary flow is produced, so the value of *Se* of the right column with VGs is larger than that of the left column without VGs. Then *Se* decreases downstream, however, when air reaches the second tube, the horseshoe vortex is generated by the tube also, secondary flow penetrated region becomes large as shown in Fig. 8(d). On the sections after the second VG and the third VG as shown in Figs. 8(e) to 8(h), it is found that the changes of *Se* are similar to the cases after the first VG as Figs. 8(c) and 8(d) except the distribution of *Se* after the second VG shown in Figs. 8(e) and 8(f) is opposite to Figs. 8(c) and 8(d). On the last section the intensity of *Se* generated by VG is weaker compared to Figs. 8(c), 8(e) and 8(g). Comparing the distributions of *Se* depicted in Fig. 8 with the distribution of longitudinal vortices on the corresponding sections in Fig. 7, it can be noticed that *Se* can well describe the intensity of longitudinal vortices on the cross sections. Comparing the secondary flow intensity with *Se* of the corresponding sections in Figs. 7 and 8, it can be found clearly that *Se* can quantify the secondary flow intensity very well in the air passage of the circle tube-finned heat exchanger.

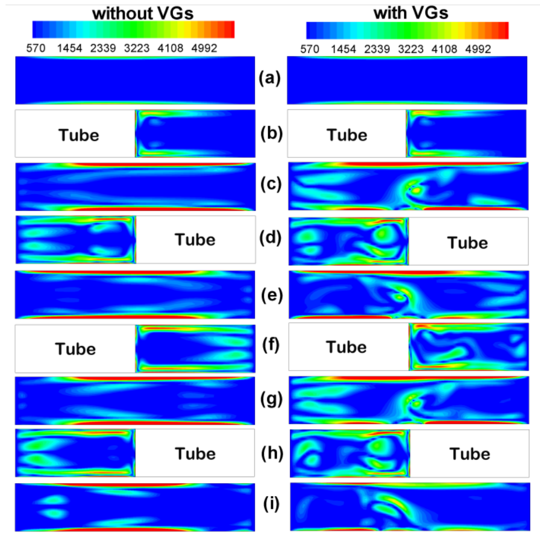

Figure 8: The distributions of *Se* on the different cross sections shown in Fig. 6 at *Re*=1134

5.2 Relationship between Nu$_s$ and Se$_s$

In order to obtain the contrastive relationships of span-averaged Nu_s and cross section averaged Se_s, the relationships of Nu_s and Se_s of some models at *Re*=1134 are shown in Fig. 9. Fig. 9(a) gives the contrastive relationship of span-averaged Nu_s and cross section averaged Se_s between the model with VGs and the model without VGs. In Fig. 9(b), we can see the relationship of Nu_s and Se_s under different transverse tube pitch. And Fig. 9(c) gives the relationship of Nu_s and Se_s under different longitudinal tube pitch. From Figs. 9(a)-9(c) we can see that for all the cases that we studied, the distribution of Nu_s has the similar variation characteristics comparing with the distribution of Se_s except at the entrance of the passage. For a detailed description of the distributions of Nu_s and Se_s and their relationship, you can see Hu et al. [Hu, Wang and Guan (2015)].

In addition, from Fig. 9(a) we can see that for the models with and without VGs under the same geometric structural parameters of tube-finned heat exchangers, the values of Nu_s almost have the same trend along the mainstream. At the entrance of fluid flow channel and at the front of each tube, there are peak values of Nu_s. And At the rear of each tube, the values of Nu_s is small. Only when VGs is introduced into the channel, the values of Nu_s increase a little downstream from the VGs, especially around the VGs there are small peaks of Nu_s. Se_s of the models with and without VGs has similar trend. The difference is that with the introduce of the VGs, the secondary flow intensity at the tube rear domain enhances, Se_s at this region increases a little. In addition, From Figs. 9(b) and 9(c), we can find when the other parameters remain the same, with increasing S_1, Se_s and Nu_s increase; with increasing S_2, Se_s and Nu_s decrease.

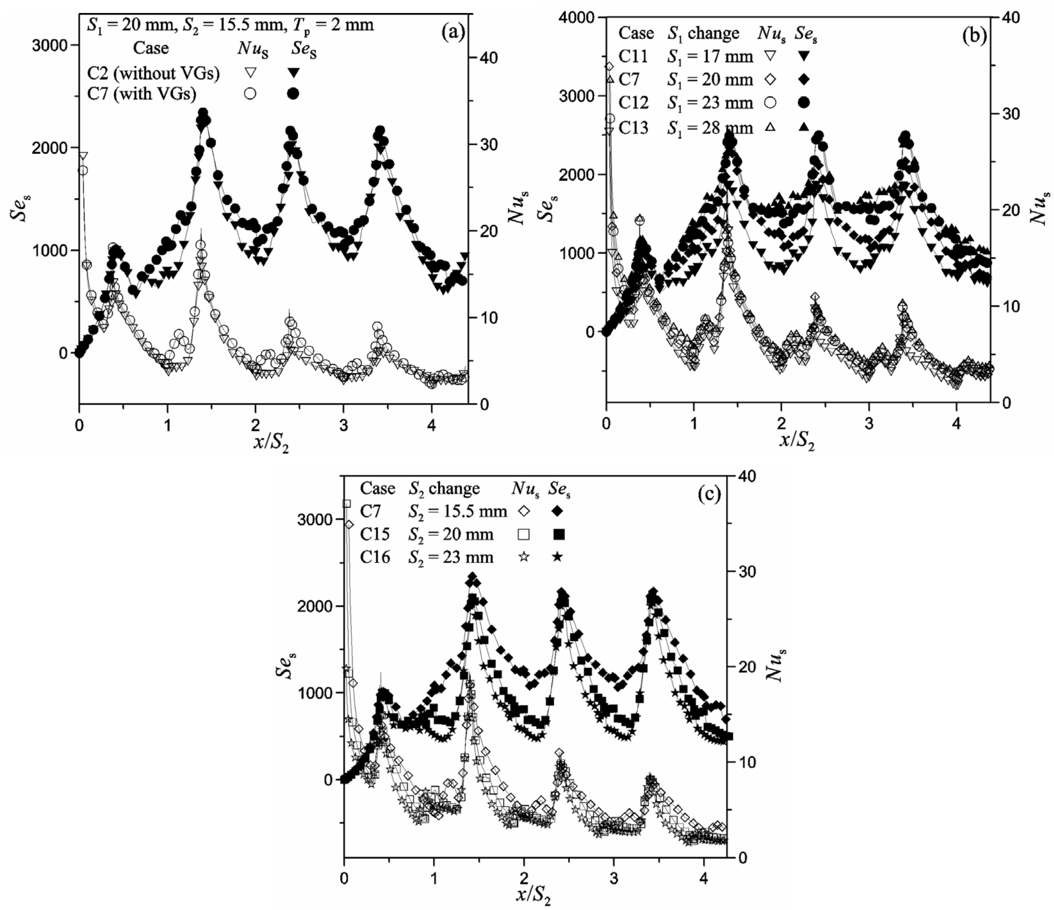

Figure 9: Comparison of Se_s and Nu_s for different cases at Re=1134

5.3 The effect of Re on Nu and Se

The relationships between *Re* and *Nu*, *Se* for all the studied cases are given in Fig. 10. As described in Fig. 10, with the increasing of *Re*, both *Se* and *Nu* increase. This indicates that with increasing of *Re*, the air velocity increases, the heat transfer of air side is enhanced and the secondary flow intensity generated by the circular tubes and VGs is increased. Through comparing Fig. 10 (a) with Fig. 10 (b), we can see that *Se* and *Nu* have almost consistent trend of change. Under the same *Re*, with the changing of configuration parameters of fin and VG, *Se* and *Nu* are all affected. For example, the C16 with S_2=23 mm has the minimum value of *Nu* and *Se*. There is little discrepancy between the C13 with S_1=28 mm and the C14 with S_2=13.5 mm. The *Nu* and *Se* values are all maximum. It is only that the effect of the changing of structural parameters on *Se* is relatively more obvious than its effect on *Nu*.

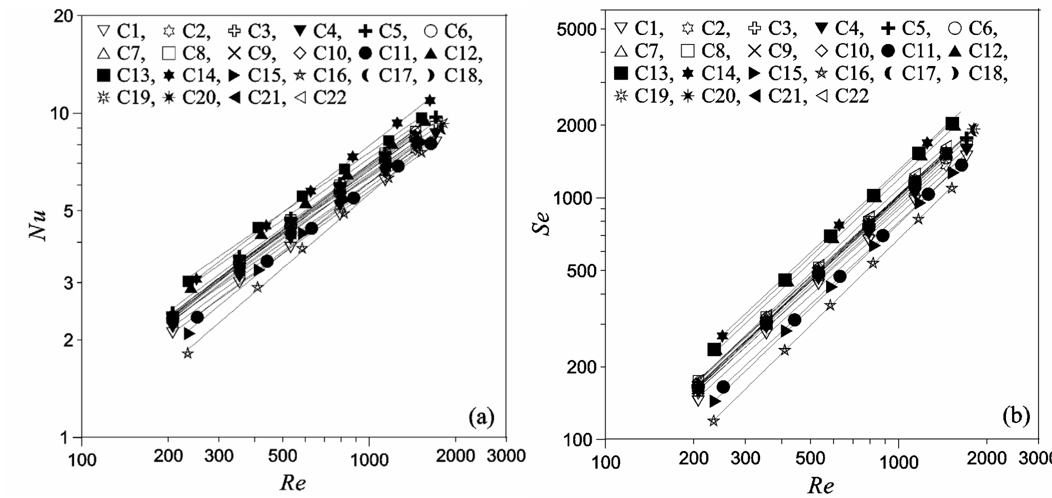

Figure 10: (a) Variation of *Nu* with *Re* among all the researched models; (b) Variation of *Se* with *Re* among all the researched models

5.4 Effect of Se on Nu

Through the above study, we can found that the *Se* can describe the secondary flow intensity in circle tube-finned heat exchanger very well. Span-averaged Nu_s and cross section averaged Se_s as well as volumetrically averaged *Se* and overall average *Nu* all have a very close connection. The effect of volumetrically averaged *Se* on overall average *Nu* for all the researched models is given in Fig. 11. From Fig. 11, we can see clearly that *Nu* increases with increasing *Se* for all the researched cases of different structural parameters, and there is one-to-one correlation between *Nu* and *Se*, that is, they have a power exponential function relationship. The fitting formula is:

$$Nu = 0.12565 Se^{0.57606} \quad (100 < Se < 3000) \tag{19}$$

Eq. (19) is only applicable to the variation range of fin and VG structural parameters that studied in this paper. The fitting line of Eq. (19) for all the simulated data is given in Fig. 10. From Fig. 10, we can see that the simulated data are in accord with the fitting line very well. Under the same *Se*, the maximum discrepancy of *Nu* between the fitting line and the simulated data is 8.8% and their mean difference is 1.1%.This implies that volumetrically averaged *Se* determines *Nu* of circle tube-finned heat exchanger.

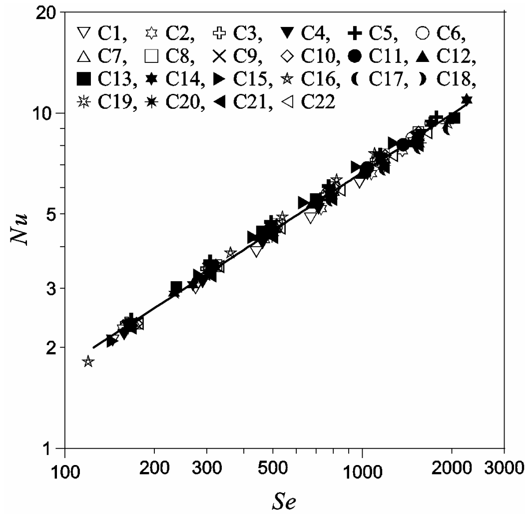

Figure 11: Variation of *Nu* with *Se* among all the researched models

5.5 Effects of Re and Se on f

Fig. 12 shows the effects of *Re* and *Se* on *f* for all the studied cases. From Fig. 12(a) we can see that for all the researched models, with the increasing of *Re*, the value of *f* is gradually decreasing. When *Re* is the same, the difference of *f* among the models with different structural parameters is apparent. The C16 with S_2=23 mm has the smallest value of *f*. When *Re* is small, *f* of the C13 with S_1=28 mm is maximum. When *Re* is large, there is little difference between the C13 with S_1=28 mm and the C14 with S_2=13.5 mm, their *f* values are maximum.

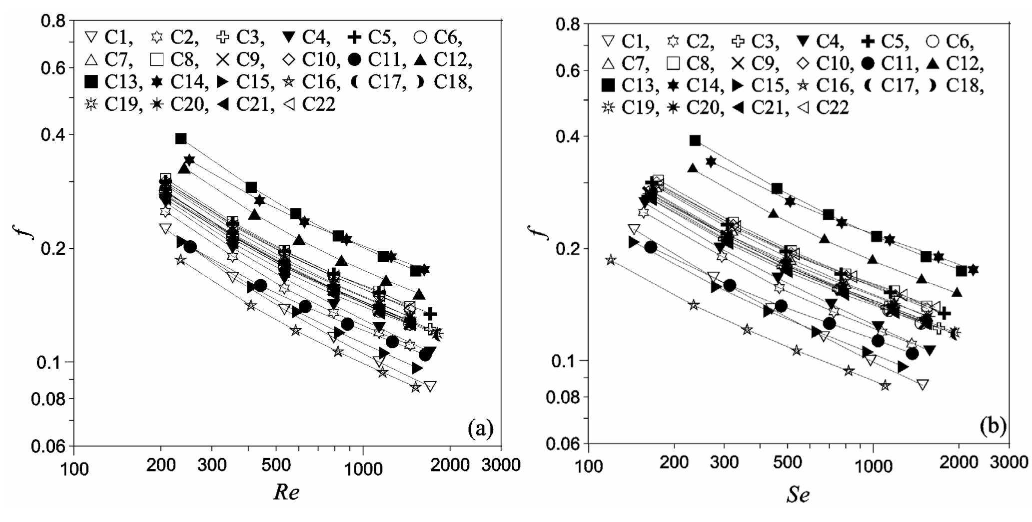

Figure 12: (a) Variation of *f* with *Re* among all the researched models; (b) Variation of *f* with *Se* among all the researched models

The effect of *Se* on *f* is given in Fig. 12(b), the trend is similar to that shown in Fig. 12(a).With the increase of *Se*, the value of *f* decreases, too. When *Se* is the same, the effect of the structural parameters change in circle tube-finned heat exchanger on *f* is relatively more obvious than the effect shown in Fig. 12(a). *f* of the C16 with S_2=23 mm is minimum. When *Se* is small, *f* of the C13 with S_1=28 mm is maximum. When *Se* is large, the difference of *f* between the C13 with S_1=28 mm and the C14 is very small and the values of *f* are maximum. Unlike the effect of *Se* on *Nu*, for all the simulated models, there is no one-to-one correlation not only between *f* and *Re* but also between *f* and *Se*. This means that *Re* and *Se* are all not the only determinant for the growth of friction coefficient. The pressure drop along the main flow direction may be mainly related to *f*, and we will do further research.

6 Conclusions

To study the effect of secondary flow intensity on heat transfer intensity and friction factor, 22 different structures of circle tube-finned heat exchanger with or without VGs were numerically studied. The dimensionless parameter *Se* is used to quantitatively describe the secondary flow intensity caused by circle tubes and vortex generators. The major corresponding conclusions are summarized below.

- *Se* can describe the secondary flow intensity induced by tubes and VGs in circle tube-finned heat exchanger very well.
- For all the cases that we studied, the span-averaged Nu_s and the cross section averaged Se_s exist nearly the same tendency except at the entrance of the passage, with the changing of configuration parameters of circle tube-finned heat exchanger, both *Nu* and *Se* are all affected.
- There is one-to-one correlation between *Nu* and *Se*, that is, there is a power exponential function relationship between *Nu* and *Se*. This implies that the volumetrically averaged *Se* is the only determining factor of *Nu* in circle tube-finned heat exchanger.
- For all the studied cases, there is no one-to-one correlation not only between *Re* and *f* but also between *Se* and *f*.

Acknowledgement: This work is supported by the National Natural Science Foundation of China (Nos. 51868035, 51866006, 51468028), Foundation of a Hundred Youth Talents Training Program of Lanzhou Jiaotong University, and the Science and Technology Plan of Gansu Province (No. 18JR3RA121).

Conflicts of Interest: The authors declare that they have no conflicts of interest to report regarding the present study.

References

Awais, M., Bhuiyan, A. A. (2019): Enhancement of thermal and hydraulic performance of compact finned-tube heat exchanger using vortex generators (VGs): a parametric study. *International Journal of Thermal Sciences*, vol. 140, pp. 154-166.

Behfard, M.; Sohankar, A. (2016): Numerical investigation for finding the appropriate design parameters of a fin-and-tube heat exchanger with delta-winglet vortex generators. *Heat and Mass Transfer*, vol. 52, no. 1, pp. 21-37.

Chang, L. M.; Wang, L. B.; Song, K. W.; Sun, D. L.; Fan, J. F. (2009): Numerical study of the relationship between heat transfer enhancement and absolute vorticity flux along main flow direction in a channel formed by a flat tube bank fin with vortex generators. *International Journal of Heat and Mass Transfer*, vol. 52, no. 7-8, pp. 1794-1801.

Delač, B.; Trp, A.; Lenić, K. (2014): Numerical investigation of heat transfer enhancement in a fin and tube heat exchanger using vortex generators. *International Journal of Heat and Mass Transfer*, vol. 78, pp. 662-669.

ElSherbini, A. I.; Jacobi, A. M. (2002): The thermal-hydraulic impact of delta-wing vortex generators on the performance of a plain-fin-and-tube heat exchanger. *HVAC&R Research*, vol. 8, no. 4, pp. 357-370.

Fiebig, M. (1995): Embedded vortices in internal flow: heat transfer and pressure loss enhancement. *International Journal of Heat and Fluid Flow*, vol. 16, no. 5, pp. 376-388.

Fiebig, M.; Valencia, A.; Mitra, N. K. (1994): Local heat transfer and flow losses in fin-and-tube heat exchangers with vortex generators: a comparison of round and flat tubes. *Experimental Thermal and Fluid Science*, vol. 8, no. 1, pp. 35-45.

Gao, S. D.; Wang, L. B.; Zhang, Y. H.; Ke, F. (2003): The optimum height of winglet vortex generators mounted on three-row flat tube bank fin. *Journal of Heat Transfer-Transactions of the ASME*, vol. 125, no. 6, pp. 1007-1016.

Gong, B.; Wang, L. B.; Lin, Z. M. (2015): Heat transfer characteristics of a circular tube bank fin heat exchanger with fins punched curve rectangular vortex generators in the wake regions of the tubes. *Applied Thermal Engineering*, vol. 75, pp. 224-238.

He, Y. L.; Chu, P.; Tao, W. Q.; Zhang, Y. W.; Tao, X. (2013): Analysis of heat transfer and pressure drop for fin-and-tube heat exchangers with rectangular winglet-type vortex generators. *Applied Thermal Engineering*, vol. 61, no. 2-3, pp. 770-783.

He, Y. L.; Han, H.; Tao, W. Q.; Zhang, Y. W. (2012): Numerical study of heat-transfer enhancement by punched winglet-type vortex generator arrays in fin-and-tube heat exchangers. *International Journal of Heat and Mass Transfer*, vol. 55, no. 21-22, pp. 5449-5458.

Hu, W. L.; Su, M.; Wang, L. C.; Zhang, Q.; Chang, L. M. et al. (2013): The optimum fin spacing of circular tube bank fin heat exchanger with vortex generators. *Heat and Mass Transfer*, vol. 49, no. 9, pp. 1271-1285.

Hu, W. L.; Song, K. W.; Guan, Y.; Chang, L. M.; Liu, S. et al. (2013): Secondary flow intensity determines Nusselt number on the fin surfaces of circle tube bank fin heat exchanger. *International Journal of Heat and Mass Transfer*, vol. 62, pp. 620-631.

Hu, W. L.; Wang, L. B.; Guan, Y. (2015): The effect of transverse tube pitch on the thermal-hydrodynamic performance of a circular tube-plate-fin heat exchanger with fin-mounted vortex generators. *Journal of Enhanced Heat Transfer*, vol. 22, no. 3, pp. 1-27.

Ke, F.; Wang, L. B.; Hua, L.; Gao, S. D.; Su, Y. X. (2006): The optimum angle of attack of delta winglet vortex generators on heat transfer performance of finned flat tube bank with considering non-uniform fin temperature. *Experimental Heat Transfer*, vol. 19, no. 3, pp.227-249.

Lemouedda, A.; Breuer, M.; Franz, E.; Botsch, T.; Delgado, A. (2010): Optimization of the angle of attack of delta-winglet vortex generators in a plate-fin-and-tube heat exchanger. *International Journal of Heat and Mass Transfer*, vol. 53, no. 23-24, pp. 5386-5399.

Lin, Z. M.; Liu, C. P.; Lin, M.; Wang, L. B. (2015): Numerical study of flow and heat transfer enhancement of circular tube bank fin heat exchanger with curved delta-winglet vortex generators. *Applied Thermal Engineering*, vol. 88, pp. 198-210.

Lin, Z. M.; Sun, D. L.; Wang, L. B. (2009): The relationship between absolute vorticity flux along the main flow and convection heat transfer in a tube inserting a twisted tape. *Heat and Mass Transfer*, vol. 45, no. 11, pp. 1351-1363.

Manglik, R. M., Bergles, A. E. (1993): Heat transfer and pressure drop correlations for twisted tape inserts in isothermal tubes: part I-Laminar flows. *Journal of Heat Transfer*, vol. 115, no. 4, pp. 881-889.

Moulin, P.; Rouch, J. C.; Serra, C.; Clifton, M. J.; Aptel, P. (1996): Mass transfer improvement by secondary flows: dean vortices in coiled tubular membranes. *Journal of Membrane Science*, vol. 114, no. 2, pp. 235-244.

Qian, Z. Q.; Wang, Q.; Cheng, J. L. (2018): Analysis of heat and resistance performance of plate fin-and-tube heat exchanger with rectangle-winglet vortex generator. *International Journal of Heat and Mass Transfer*, vol. 124, pp. 1198-1211.

Salleh, M. F. M.; Gholami, A.; Wahid, M. A. (2019): Numerical evaluation of thermal hydraulic performance in fin-and-tube heat exchangers with various vortex generator geometries arranged in common-flow-down or common-flow-up. *Journal of Heat Transfer-Transactions of the ASME*, vol. 141, no. 2, 021801.

Salviano, L. O.; Dezan, D. J.; Yanagihara, J. I. (2016): Thermal-hydraulic performance optimization of inline and staggered fin-tube compact heat exchangers applying longitudinal vortex generators. *Applied Thermal Engineering*, vol. 95, pp. 311-329.

Sarangi, S. K.; Mishra, D. P. (2017): Effect of winglet location on heat transfer of a fin-and-tube heat exchanger. *Applied Thermal Engineering*, vol. 116, pp. 528-540.

Song, K. W.; Hu, W. L.; Liu, S.; Wang, L. B. (2016): Quantitative relationship between secondary flow intensity and heat transfer intensity in flat-tube-and-fin air heat exchanger with vortex generators. *Applied Thermal Engineering*, vol. 103, pp. 1064-1070.

Song, K. W.; Wang, L. B. (2013): The effectiveness of secondary flow produced by vortex generators mounted on both surfaces of the fin to enhance heat transfer in a flat tube bank fin heat exchanger. *Journal of Heat Transfer-Transactions of the ASME*, vol. 135, no. 4, 041902.

Song, K. W.; Xi, Z. P.; Su, M.; Wang, L. C.; Wu, X. et al. (2017): Effect of geometric size of curved delta winglet vortex generators and tube pitch on heat transfer characteristics of fin-tube heat exchanger. *Experimental Thermal and Fluid Science*, vol. 82, pp. 8-18.

Wang, L. C.; Su, M.; Hu, W. L.; Lin, Z. M.; Wang, Y. (2011): The characteristic temperature in the definition of heat transfer coefficient on the fin side surface in tube bank fin heat exchanger. *Numerical Heat Transfer Part A-Applications*, vol. 60, no. 10, pp. 848-866.

Zhang, Y. H.; Wang, L. B.; Yang, S. C. (2003): Effect of parameters of vortex generator on local heat transfer performance of tube-fin heat exchanger. *Journal of Industrial and Engineering Chemistry*, vol. 54, no. 3, pp. 294-298.

Zhang, Y. H.; Wu, X.; Wang, L. B. (2008): Comparison of heat transfer performance of tube bank fin with mounted vortex generators to tube bank fin with punched vortex generators. *Experimental Thermal and Fluid Science*, vol. 33, no. 1, pp. 58-66.